

# Controlling Magnetization Vector Depth Profiles of $\text{La}_{0.7}\text{Sr}_{0.3}\text{CoO}_3/\text{La}_{0.7}\text{Sr}_{0.3}\text{MnO}_3$ Exchange Spring Bilayers via Interface Reconstruction

*‡Alexander M. Kane<sup>1</sup>, I-Ting Chiu<sup>1</sup>, Nolan J. Ahlm<sup>1</sup>, Rajesh V. Chopdekar<sup>1,2</sup>, Alpha T. N'Diaye<sup>2</sup>, Elke Arenholz<sup>2,3</sup>, Apurva Mehta<sup>4</sup>, ‡Valeria Lauter<sup>5</sup> and ‡\*Yayoi Takamura<sup>1</sup>*

<sup>1</sup>Department of Materials Science and Engineering, University of California, Davis, Davis, California 95616, USA

<sup>2</sup>Advanced Light Source, Lawrence Berkeley National Laboratory, Berkeley, California 94720, USA

<sup>3</sup>Cornell High Energy Synchrotron Source, Cornell University, Ithaca, New York 14853

<sup>4</sup>Stanford Synchrotron Radiation Lightsource, SLAC National Accelerator Laboratory, Menlo Park, California 94025, USA

<sup>5</sup>Spallation Neutron Source, Oak Ridge National Laboratory, Oak Ridge, Tennessee 37830, USA

Keywords: Magnetism, Exchange Bias, Perovskites, Thin Films, Charge Transfer, Interface Reconstruction, Polarized Neutron Reflectometry.

Abstract:

The  $\text{La}_{0.7}\text{Sr}_{0.3}\text{CoO}_{3-\square}$  /  $\text{La}_{0.7}\text{Sr}_{0.3}\text{MnO}_{3-\square}$  (LSCO/LSMO) bilayer system is an ideal perovskite oxide platform for investigating electronic interface reconstruction and its effect on the magnetic properties. Previous studies have shown LSCO can separate into magnetic sublayers which possess distinct trends as the total LSCO thickness increases. In this study we used polarized neutron reflectometry to quantify changes to the magnetic and chemical depth profiles and it confirms the formation of  $\sim 12 \text{ \AA}$  thick interfacial LSCO and LSMO layers, characterized by a decreased nuclear scattering length density compared to the bulk of the layers. This decrease is attributed to the combined effects of oxygen vacancy formation and interfacial charge transfer which lead to magnetically active  $\text{Co}^{2+}$  ions with ionic radii larger than the  $\text{Co}^{3+}/\text{Co}^{4+}$  ions typically found in bulk LSCO or single layer films. The interfacial magnetization values, as well as  $\text{Co}^{2+}$  ion and oxygen vacancy concentrations, depend strongly on the LSCO layer thickness. These results highlight the sensitive interplay of the cation valence states, oxygen vacancy concentration, and magnetization at interfaces in perovskite oxide multilayers, demonstrating the potential to tune their functional properties via careful design of their structure.

## Introduction:

Perovskite oxides have received significant interest for applications in next-generation magnetic and ferroelectric devices due to their tunable charge, spin, lattice, and orbital degrees of freedom that provide remarkable sensitivity to external stimuli.<sup>1</sup> In particular, interfaces in multilayers have been shown to drive charge transfer reactions and unexpected phenomena that are not observed in the constituent materials.<sup>2-5</sup> Exchange spring magnets, bilayers composed of hard/soft magnetic materials, have been studied intensely for their use as permanent magnets<sup>6,7</sup> and in heat-assisted magnetic recording devices.<sup>8,9</sup> Most exchange spring research has been focused on metal bilayers, but an all-oxide exchange spring could provide a degree of tunability absent in the purely metallic counterparts. One example is the perovskite exchange spring bilayer comprised of  $\text{La}_{0.7}\text{Sr}_{0.3}\text{CoO}_{3-\square}$  and  $\text{La}_{0.7}\text{Sr}_{0.3}\text{MnO}_{3-\square}$  (LSCO/LSMO), hard and soft ferromagnetic (FM) layers respectively. In this system, an interfacial layer characterized by magnetically active  $\text{Co}^{2+}$  ions (s-LSCO) couples to, and switches concurrently with, the soft LSMO layer.<sup>10,11</sup> Previous studies have suggested that for LSCO thicknesses greater than  $\sim 50$  Å, beneath the s-LSCO layer, the remaining LSCO layer maintains the expected  $\text{Co}^{3+}/\text{Co}^{4+}$  valence state and hard FM behavior of single layer films (h-LSCO). The h-LSCO layer imposes a reversible exchange bias (EB) shift in the coupled soft layers in a direction opposite to the bias field. A detailed spectroscopy study as a function of LSCO layer thickness demonstrated that the  $\text{Co}^{2+}$  ion concentration is inversely related to the total LSCO thickness.<sup>12</sup> However, these prior studies were unable to quantitatively determine the interface layer magnetization and thickness, the role

of oxygen vacancies, and whether magnetization reversal proceeds via a gradual unwinding as with metallic exchange springs or via domain nucleation within the soft layer.

To address these questions, we used polarized neutron reflectometry (PNR) which combines the depth sensitivity of thin film reflectivity experiments with the magnetization dependent scattering of polarized neutrons, as well as the capability to quantify changes in oxygen content from nuclear scattering that is typically difficult due to its low atomic mass.<sup>13-16</sup> Among a variety of magnetic systems, this technique has been used to map the chiral magnetic structure of metallic exchange spring multilayers including the SmCo/Fe,<sup>17</sup> CoFe<sub>2</sub>O<sub>4</sub>/CoFe<sub>10</sub>,<sup>18</sup> Fe/Cr,<sup>19</sup> and Fe<sub>55</sub>Pt<sub>45</sub>/Ni<sub>80</sub>Fe<sub>20</sub><sup>20</sup> systems. It has also attracted intense interest in the study of perovskite thin films and multilayers, owing to their unusual magnetic behavior produced by interfacial electronic reconstruction. Hoffman *et al.* revealed that a noncollinear magnetic structure existed between successive LSMO layers in (LaNiO<sub>3</sub>)<sub>n</sub>/(LSMO)<sub>9</sub> superlattices (*n* is # of unit cells), which they attributed to charge transfer at the LaNiO<sub>3</sub>/LSMO interface and Ni<sup>2+</sup> ions that couple to the LSMO layers.<sup>21,22</sup> Furthermore, *in-situ* measurements of magnetic depth profiles in ion gelled La<sub>0.5</sub>Sr<sub>0.5</sub>CoO<sub>3- $\delta$</sub>  films correlated a decrease in magnetization to gating-induced oxygen vacancy formation.<sup>23</sup> Gilbert *et al.* investigated oxygen vacancies introduced in Gd-capped LSCO films, which produced a spontaneous redox reaction at room temperature to form GdO<sub>x</sub> and led to degraded magnetic properties and a topotactic phase transition to the La<sub>0.7</sub>Sr<sub>0.3</sub>CoO<sub>2.5</sub> brownmillerite structure.<sup>24,25</sup> These examples highlight the need of a depth-sensitive probe like neutron reflectometry to help unravel emergent interfacial phenomena and nanoscale magnetic variations in systems similar to the LSCO/LSMO bilayers investigated here.

The PNR measurements were combined with bulk magnetometry and soft x-ray magnetic spectroscopy to quantitatively describe changes to the chemical and magnetic depth profiles in two LSCO/LSMO bilayers resulting from electronic interface reconstruction. Two bilayers with different LSCO layer thicknesses were chosen to investigate the two switching regimes indicated from previous studies of this system<sup>11</sup>: the single phase magnetic reversal when the LSCO thickness is below  $\sim 50$  Å and the two-phase reversal exchange biased regime for thicker LSCO layers. The PNR measurements reveal that the charge transfer interfacial layers of  $\sim 12$  Å possess decreased nuclear scattering length density compared to the bulk of the layers on both sides of the LSCO/LSMO interface. These results explain that the magnetization of the s-LSCO sublayer depends strongly on the LSCO thickness due to changes in the  $\text{Co}^{2+}$  ion and oxygen vacancy concentrations.

### **Experimental Section:**

The LSCO/LSMO exchange spring bilayers were grown on (001)-oriented  $(\text{LaAlO}_3)_{0.3}(\text{Sr}_2\text{TaAlO}_6)_{0.7}$  (LSAT) substrates by pulsed laser deposition. The designed LSCO layer thicknesses were 40 and 80 Å, each capped with 60 Å of LSMO, referred to as samples C4M6 and C8M6, respectively. Therefore, the bilayers investigated here bridge the critical LSCO thickness needed to observe EB from the h-LSCO layer. The bilayers were grown at a substrate temperature of 700 °C in 300 mTorr  $\text{O}_2$  pressure, using a KrF (248 nm) excimer laser at 0.9 J/cm<sup>2</sup> fluence and 1 Hz repetition rate. The samples were cooled to room temperature in 300 Torr  $\text{O}_2$  to ensure proper oxygen content within the bilayer.

The structural properties of the films were characterized by x-ray reflectivity (XRR), high-resolution  $\omega$ - $2\theta$  scans, and reciprocal space maps (RSMs) in a Bruker D8 Discover x-ray diffractometer using Cu  $K\alpha_1$  x-rays. They were further characterized using resonant x-ray reflectivity (RXRR) measurements at beamline 2-1 of the Stanford Synchrotron Radiation Lightsource at SLAC National Accelerator Laboratory. RXRR profiles were measured at the Co and Mn  $K$ -edges and an off-resonant energy (8 keV). By tuning to the resonant energies of the B-site ions, we improve the scattering length density (SLD) contrast between perovskite oxide layers of similar chemical density.<sup>26</sup> All three energies were fit simultaneously to one structural model using GenX reflectivity software,<sup>27</sup> where atomic scattering factors were selected as additional fit parameters to account for on-resonance variations to the SLD. A carbon surface layer was added to the sample model due to prolonged sample exposure to hard x-rays in air.

The bulk magnetic properties were investigated using a Quantum Design VersaLab physical properties measurement system. Minor hysteresis loops were measured to  $\pm 0.4$  T after biasing the sample with  $\pm 3$  T. Magnetization values were calculated based on the total layer thicknesses of the bilayers. The magnetic/electronic structure was probed using x-ray absorption and x-ray magnetic circular dichroism (XA/XMCD) spectroscopy at beamline 4.0.2 of the Advanced Light Source (ALS) at Lawrence Berkeley National Laboratory. To ensure the saturation of the h-LSCO layer, the samples were field cooled in 0.3 T and XMCD measurements were taken with a fixed field of 0.3 T and alternating circular polarization of the x-rays. Two detection methods were used: total electron yield (TEY) which provides surface sensitive measurements of the top 4-10 nm of the sample,<sup>28</sup> and luminescence yield (LY), which probes the full thickness of the film stack.<sup>29</sup> Therefore, Co-TEY measurements primarily probe the s-LSCO layer at the

LSCO/LSMO interface, while Co-LY measurements are well-suited to probe the buried h-LSCO layer. All magnetic and spectroscopy measurements were performed at 80 K.

PNR measurements were performed at the Magnetism Reflectometer (Beamline 4A) of the Spallation Neutron Source (SNS) at Oak Ridge National Laboratory<sup>30</sup> using the time of flight method and a neutron wavelength band of 2-5 Å. Bilayer C4M6 was measured in a saturating field of 1.1 T, while bilayer C8M6 was field cooled in -1.1 T to saturate all magnetic layers, followed by measurement in 0.2 T and 1.1 T, corresponding to antiparallel and parallel alignments of the hard/soft magnetic layers, respectively.  $R^+$  and  $R^-$  spin channels were measured, which correspond to initial up/down neutron polarization, respectively, and the data was co-refined simultaneously in GenX<sup>27</sup> with XRR data.

### **Results and Discussion:**

RXRR data and fits for the three x-ray energies are shown in Figure S1 for both bilayers and the fit parameters are given in Tables ~~SI~~ S1 and ~~SH~~ S2. Best fits were obtained using a structural model that separates both the LSMO and LSCO layers into two sublayers with interface roughness  $\leq 5$  Å, indicating that the bilayers possess smooth structural interfaces with minimal chemical intermixing.  $\omega$ - $2\theta$  scans (Figure S2) display clear thickness fringes indicating that the bilayers possess a high degree of structural coherence in the out-of-plane direction. Fitting was performed using Bruker Leptos software,<sup>31</sup> and fit parameters are listed in Table ~~SHI~~ S3. The layer thicknesses are in reasonable agreement with the designed values, and both film layers are coherently strained to the LSAT substrate as demonstrated by the reciprocal space maps in Figure S3.

The bulk magnetic hysteresis loops of the two bilayers (Figure 1(a)) display the expected behavior for LSCO/LSMO bilayers with LSCO layer thicknesses which bridge the critical LSCO thickness for EB from the h-LSCO layer.<sup>10-12</sup> Bilayer C4M6 displays a single, sharp transition due to the magnetic coupling of the s-LSCO and LSMO layers, while bilayer C8M6 shows two magnetic transitions from the h-LSCO layer and the coupled soft layers. As a result, bilayer C8M6 displays an EB shift (Figure 1(b)) in the biased minor loops characteristic of exchange spring systems. The minor hysteresis loops have been centered vertically to remove the shift due to the saturated h-LSCO layer not reversed by 0.1 T magnetic fields.

Further insight into the magnetic behavior can be obtained from the Co-XA/XMCD spectra for the bilayers (Figure 1(c) and (d) with reference spectra for Co<sup>2+</sup> ions (La<sub>2</sub>CoMnO<sub>6</sub> (LCMO)) and Co<sup>3+</sup>/Co<sup>4+</sup> ions (LSCO) included). While the differences in the shapes of the XA spectra between bilayers and comparing TEY and LY detection modes are subtle, notable differences exist in the XMCD spectra. For bilayer C4M6, a strong XMCD signal closely resembling the Co<sup>2+</sup> reference spectrum is observed only for the TEY detection mode confirming the presence of magnetically active Co<sup>2+</sup> ions in the interfacial s-LSCO layer. The signature of Co<sup>2+</sup> ions is also present in the TEY XA spectrum (features indicated by the vertical black dashed lines), while the corresponding LY XA spectrum is dominated by signatures of mixed Co<sup>3+</sup>/Co<sup>4+</sup> ions indicating that a weakly magnetic LSCO layer lies at the LSAT substrate interface. In contrast, the dominant XMCD signal for bilayer C8M6 is observed with the LY detection mode with characteristics dominated by mixed Co<sup>3+</sup>/Co<sup>4+</sup> ions of the h-LSCO layer. The TEY data exhibits an 85% decrease in XMCD peak intensity compared to the LY data and has nearly equal

contributions from  $\text{Co}^{2+}$  and  $\text{Co}^{3+}/\text{Co}^{4+}$  type FM ordering. A slight shift of the main Co  $L_3$  peak to lower energy in the TEY spectrum compared to the LY spectrum corroborates the presence of  $\text{Co}^{2+}$  ions at the LSCO/LSMO interface. Therefore, the magnetization of the s-LSCO layer decreases as the LSCO thickness increases due to the presence of the h-LSCO layer.<sup>12</sup>

The Mn spectra (Figure S4) resemble single-layer LSMO films for both bilayers. The main Mn  $L_3$  peak in the LY spectra are shifted to slightly higher photon energies, indicative of a higher  $\text{Mn}^{4+}$  to  $\text{Mn}^{3+}$  ratio and consistent with charge transfer at the LSCO/LSMO interface.<sup>10</sup> The TEY XMCD peak intensity is 20% smaller than the LY data, likely due to a surface layer of reduced magnetization commonly observed in LSMO films.<sup>32-36</sup>

To clarify the relationship between total LSCO thickness, its constituent sublayer thicknesses and magnetization, and oxygen content, we next address the PNR data. Figure 2(a) plots this data for bilayer C4M6, where the splitting between the two spin channels indicates FM order. The best fits consisted of a model with two LSCO layers: the main layer at substrate interface and the s-LSCO layer; and three LSMO layers: the interface layer with increased  $\text{Mn}^{4+}$  concentration, the main LSMO layer, and the surface layer of reduced magnetization.<sup>32,33</sup> The nuclear SLD from this fit (Figure 2(b)) indicates the formation of thin layers (12 Å or three unit cells) with a decrease in the nuclear SLD on either side of the LSCO/LSMO interface; 3.9% and 3.3% decrease for interface LSCO and LSMO layers, respectively. The densities of the main layers are consistent with theoretical density. The thickness of these interface layers are consistent with that reported for charge transfer layers at oxide interfaces.<sup>2,37</sup> The reduced density likely results from the large ionic radius of  $\text{Co}^{2+}$  ions compared to  $\text{Co}^{3+}/\text{Co}^{4+}$  ions (18-32% larger for high spin state

configurations),<sup>38,39</sup> and possibly the presence of oxygen vacancies.<sup>40-42</sup> Attributing this density loss solely to oxygen vacancies places upper bounds of oxygen nonstoichiometry at the interface at  $\delta = 0.20 \pm 0.01$  for the LSCO and LSMO interface layers.<sup>43</sup> To confirm the sensitivity of the PNR model to the decrease in density for the interfacial layers, alternative fits are presented in Figures S5-S6 for bilayer C4M6, each of which provides an inferior fit to the measured data. The corresponding sample magnetization indicates that the main LSCO layer retains a small magnetic moment ( $0.4 \mu_B/\text{Co ion}$  or  $66 \text{ emu/cm}^3$ ) compared to  $\sim 0.9 \mu_B/\text{Co ion}$  ( $150 \text{ emu/cm}^3$ ) for bulk LSCO,<sup>44</sup> while the s-LSCO layer has a much larger moment of  $1.46 \mu_B/\text{Co ion}$  ( $240 \text{ emu/cm}^3$ ). The magnetizations of the interface, main, and surface LSMO sublayers are  $3.4 \mu_B/\text{Mn ion}$  ( $538 \text{ emu/cm}^3$ ),  $3.7 \mu_B/\text{Mn ion}$  ( $586 \text{ emu/cm}^3$ ), and  $0.52 \mu_B/\text{Mn}$  ( $80 \text{ emu/cm}^3$ ), respectively, where the magnetization of the main layer is consistent with bulk values.<sup>45</sup> By comparing the magnetization values obtained from the PNR fits to the bulk magnetization data, described in greater detail in the supporting information, we estimate the individual layer magnetization values to be within  $\pm 15$ – $20\%$  of the neutron fit values, and the magnetization trends are consistent across all measurement techniques.

While bilayer C4M6 exhibited an LSCO interface layer with magnetization larger than bulk values, the PNR data and SLD profiles for bilayer C8M6 shown in Figure 3 exhibit the opposite behavior. Best fits were obtained using a similar model as bilayer C4M6 with an additional  $4 \text{ \AA}$  nonmagnetic LSCO layer at the LSAT/LSCO interface<sup>46</sup> such that the LSMO and LSCO layers are both broken up into three sublayers. The LSCO and LSMO interface layers maintain a thickness of  $\sim 12 \text{ \AA}$  with a 3.1% and 1.6% nuclear SLD reduction for the interface-LSCO and

LSMO layers, respectively. These densities correspond to upper bounds on oxygen nonstoichiometry of  $\delta = 0.09 \pm 0.01$ . A fit with fixed nSLD for all LSCO layers is presented in Figure S7, which shows larger deviation from the measured data compared to the fit with decreased density for the interfacial layers. The s-LSCO and h-LSCO layers have magnetizations of  $0.29 \mu_B/\text{Co}$  and  $1.16 \mu_B/\text{Co}$  ion, respectively. For the LSMO layer, the oxygen vacancies and charge transfer model produce counteracting effects on the Mn valence state; oxygen vacancies produce excess negative charge and thus a greater proportion of  $\text{Mn}^{3+}$  ions, while interfacial charge transfer between Co and Mn ions favors the formation of  $\text{Mn}^{4+}$  ions. The Mn XA spectra for the bilayers are consistent with these counteracting mechanisms, as they show minimal deviation from a LSMO thin film.

In comparison to bilayer C4M6, the magnetization of the s-LSCO layer is significantly decreased, while that of the h-LSCO layer is enhanced, in agreement with the TEY/LY Co-XMCD signals for this bilayer. The magnetizations of the interface, main, and surface LSMO sublayers are 2.41, 2.91, and  $0.27 \mu_B/\text{Mn}$  ion, in reasonable agreement with those of bilayer C4M6. The difference in LSMO magnetization compared to C4M6 is likely attributed to an increase in  $\text{Mn}^{4+}$  ion concentration which is expected to decrease the magnetization, an assertion supported by the Mn spectroscopy data in Figure S4. The as-designed LSMO is near the optimal doping limit for maximized magnetization and  $T_C$ ,<sup>47</sup> and an increase in  $\text{Mn}^{4+}$  to  $\text{Mn}^{3+}$  ratio effectively shifts the LSMO to higher Sr doping and leaves fewer 3d electrons to contribute to the magnetization. Furthermore, the magnetization profile indicates the antiparallel alignment of the h-LSCO and s-LSCO/LSMO layers at 0.2 T, with negative magnetization within the h-LSCO layer and no component of the magnetization perpendicular to the field direction. Therefore,

magnetization reversal is likely driven by domain nucleation in the LSMO layer parallel to the magnetic field, which switches the s-LSCO layer through interfacial coupling, rather than through a helical magnetic structure at the magnetic interface.

The magnetization depth profiles obtained from PNR measurements provide further information for our interface model of the LSCO thickness dependence of the magnetic behavior of LSCO/LSMO bilayers.<sup>12</sup> According to this model, the LSCO and LSMO layers break up into multiple sublayers with differing density, electronic structure, and magnetic properties. Charge transfer occurs across the LSCO/LSMO interface forming two interface layers of  $\sim 12$  Å thickness with increased  $\text{Co}^{2+}$  and  $\text{Mn}^{4+}$  ion concentrations, respectively, and with reduced densities compared to bulk values. Within the resolution of our measurements, the thickness of the interface layers is independent of LSCO thickness. On the LSMO side of the bilayer, the interfacial LSMO sublayer has suppressed magnetization, consistent with oxygen deficient LSMO and an increase in the  $\text{Mn}^{4+}/\text{Mn}^{3+}$  ratio,<sup>35,48,49</sup> while the main and surface LSMO sublayers behave as expected for LSMO thin films.<sup>32-36</sup>

However, the behavior is more complex on the LSCO side of the bilayer. The s-LSCO layer is characterized by magnetically active  $\text{Co}^{2+}$  ions which couple to the soft LSMO layer. As the LSCO layer thickness increases, the  $\text{Co}^{2+}$  ion concentration and XMCD contribution in the s-LSCO layer decrease, leading to a decrease in the s-LSCO magnetization, while the h-LSCO layer coercivity and magnetization gradually increase. As a result, a critical LSCO thickness of  $\sim 50$  Å exists, above which a distinct h-LSCO layer forms and which imposes a reversible EB shift in the coupled soft layers. Below the critical thickness, the s-LSCO layer is dominated by the

magnetically active  $\text{Co}^{2+}$  ions leading to a large magnetization ( $1.46 \mu_{\text{B}}/\text{Co}$  ion) and reduced density due to the relative  $\text{Co}^{2+}/\text{Co}^{3+}/\text{Co}^{4+}$  ionic radii. In contrast, above the critical thickness, the  $\text{Co}^{3+}/\text{Co}^{4+}$  ions that replace  $\text{Co}^{2+}$  ions in the s-LSCO layer do not contribute significantly to its magnetization, despite a valence state closely resembling that of bulk LSCO which might suggest a bulk-like moment. We believe that this is due to the limited number of  $\text{Co}^{2+}$  ions which disrupt the double exchange mechanism between  $\text{Co}^{3+}/\text{Co}^{4+}$  ions. The resulting s-LSCO magnetization lies below that of bulk LSCO, suggesting that the reduced density in this case occurs more due to oxygen vacancies at the interface, as the larger  $\text{Co}^{2+}$  ions comprise a much smaller percentage of interface Co ions. It should be noted that the small lattice mismatch between LSCO and LSAT (0.61% tensile strain) is expected to limit the driving force for the formation of ordered oxygen vacancies observed in cobaltite thin films,<sup>50</sup> such that we do not expect to form a significant amount of brownmillerite phase within the cobaltite layer.

## **Conclusion:**

In summary, we present a comprehensive interface model to explain the LSCO thickness dependence of the magnetic behavior of LSCO/LSMO bilayers. We determine that the length scale of electronic reconstruction in the form of charge transfer extends  $\sim 12 \text{ \AA}$  from either side of the LSCO/LSMO interface. These interface layers are characterized by reduced density and increased  $\text{Co}^{2+}$  and  $\text{Mn}^{4+}$  ion concentrations, respectively, compared to the bulk of the layers. The magnetization values of the LSCO sublayers depend strongly on the LSCO thickness: the s-LSCO magnetization decreases from  $1.46$  to  $0.30 \mu_{\text{B}}/\text{Co}$  ion for LSCO thicknesses of  $40$  and  $80 \text{ \AA}$ , respectively, while the h-LSCO magnetization increases from  $0.4$  to  $1.16 \mu_{\text{B}}/\text{Co}$  ion, with a

corresponding increase in coercivity. These trends result from a gradual decrease in the concentration of magnetically active  $\text{Co}^{2+}$  ions in the s-LSCO layer, as well as the presence of oxygen vacancies. As a result, a critical thickness of  $\sim 50 \text{ \AA}$  exists, above which the h-LSCO layer forms and which can impose EB to the coupled s-LSCO/LSMO soft layers. These results highlight the interplay of charge transfer and oxygen stoichiometry in altering the magnetic profiles of perovskite oxide multilayers and provide a route to tune their functional properties via careful design of their structure.

## FIGURES

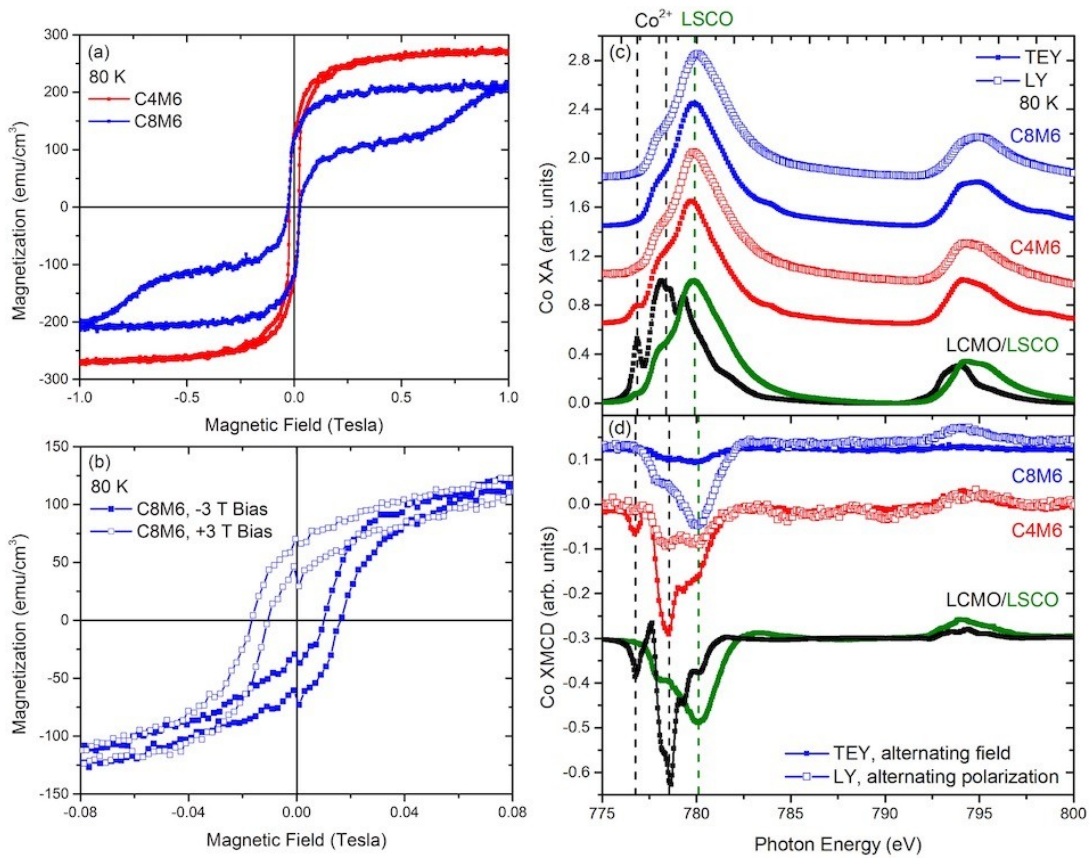


**Figure 1.** Bulk magnetization (a) major hysteresis loops and (b) biased minor hysteresis loops. The minor hysteresis loops have been centered vertically to remove the shift due to the saturated h-LSCO layer not reversed by 0.1 T magnetic fields. (c) Co-XA and (d) Co-XMCD spectra closed/open symbols correspond to TEY/LY detection. LY Co-XMCD spectra were collected with fixed field and alternating circular polarization after field cooling in 0.3 T, while TEY Co-XMCD spectra were taken with  $\pm 0.3$  T and fixed circular polarization. Black and green curves correspond to  $\text{Co}^{2+}$  and  $\text{Co}^{3+}/\text{Co}^{4+}$  reference spectra, respectively.

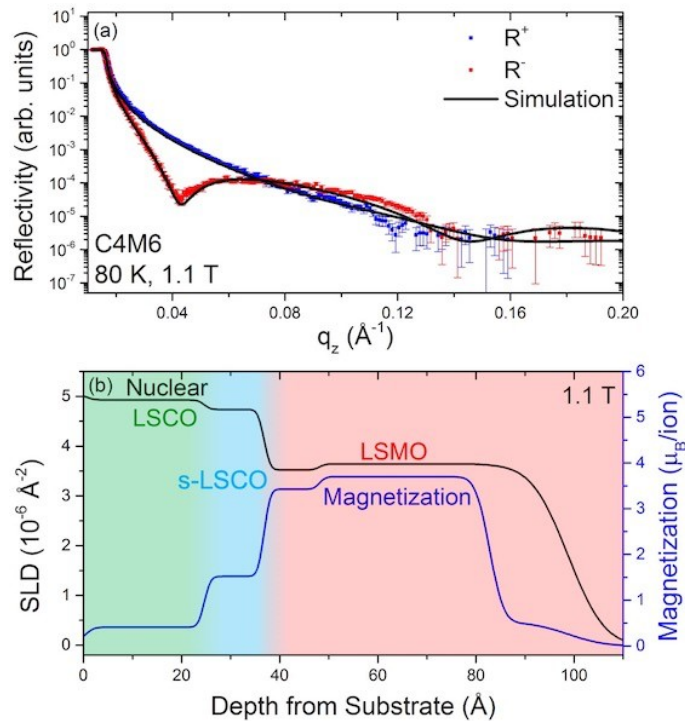


**Figure 2.** (a) Simultaneous PNR fits at 1.1 T and (b) nuclear SLD and magnetization profiles for bilayer C4M6.

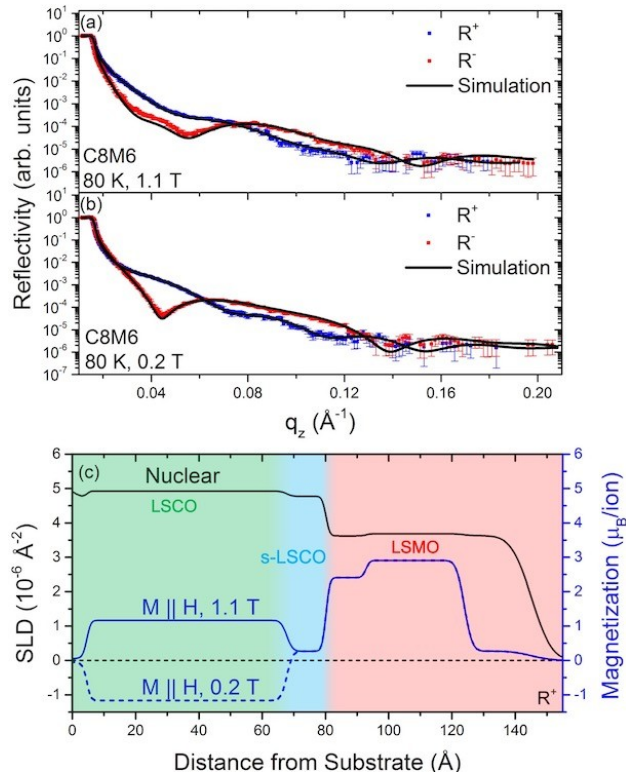
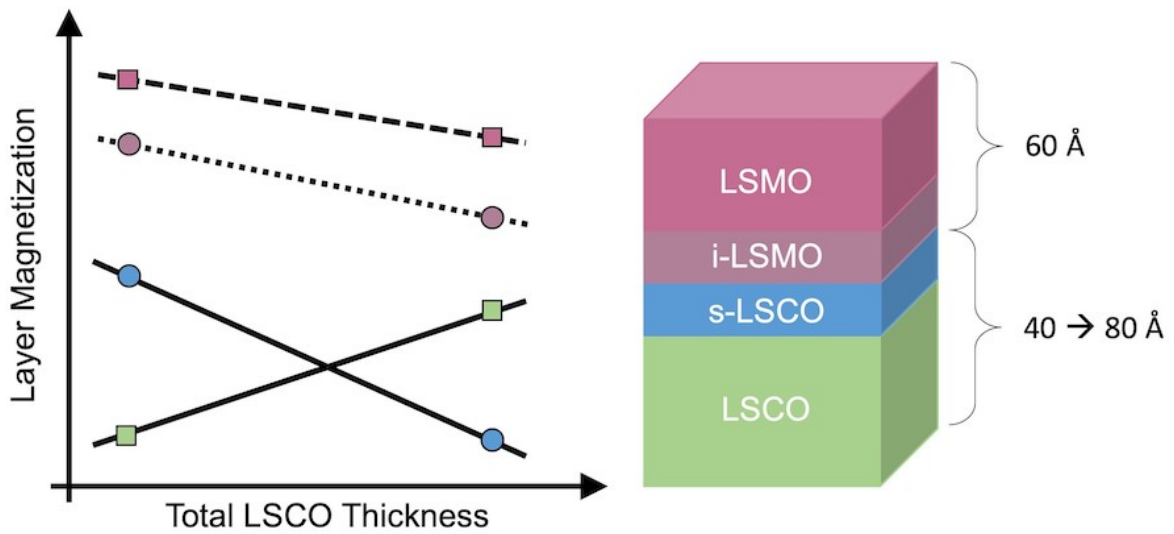


**Figure 3.** PNR data and fits for bilayer C8M6 at (a) 1.1 T and (b) 0.2 T after an initial field cooling in -1.1 T. (c) Nuclear SLD and magnetization depth profiles.



**TOC Figure.**

## ASSOCIATED CONTENT

### **Supporting Information.**

The following files are available free of charge.

Structural characterization and Mn spectroscopy data can be found in the following supporting information PDF file: LSCOThicknessNeutronpaper\_Supplemental\_v3.pdf

## AUTHOR INFORMATION

### **Corresponding Author**

\*Yayoi Takamura, ytakamura@ucdavis.edu

### **Author Contributions**

The manuscript was written through contributions of all authors. All authors have given approval to the final version of the manuscript. ‡These authors contributed equally.

### **Funding Sources**

Financial support for this project was provided by the University of California, Multicampus Research Programs and Initiatives grant MR-15-328528, National Science Foundation grant DMR - 1745450, and the U.S. Department of Energy (DOE), Office of Science, Office of Workforce Development for Teachers and Scientists, Office of Science Graduate Student Research (SCGSR) program. The SCGSR program is administered by the Oak Ridge Institute for Science and Education (ORISE) for the DOE. ORISE is managed by Oak Ridge Associated Universities under contract number DE-SC0014664. This research used resources of the ALS, which is a DOE Office of Science User Facility under contract No. DE-AC02-05CH1123. Use of SSRL, SLAC National Accelerator Laboratory, is supported by the U.S. DOE, Office of Science,

Office of Basic Energy Sciences under Contract No. DE-AC02-76SF00515. The research performed at ORNL's Spallation Neutron Source was sponsored by the Scientific User Facilities Division, Office of Basic Energy Sciences, U.S. Department of Energy.

## REFERENCES

- (1) Dagotto, E.; Hotta, T.; Moreo, A. Colossal Magnetoresistant Materials: The Key Role of Phase Separation. *Physics Reports* **2001**, *344* (1–3), 1–153. [https://doi.org/10.1016/S0370-1573\(00\)00121-6](https://doi.org/10.1016/S0370-1573(00)00121-6).
- (2) Ohtomo, A.; Muller, D. A.; Grazul, J. L.; Hwang, H. Y. Artificial Charge-Modulation in Atomic-Scale Perovskite Titanate Superlattices. *Nature* **2002**, *419* (6905), 378–380. <https://doi.org/10.1038/nature00977>.
- (3) Ohtomo, A.; Hwang, H. Y. A High-Mobility Electron Gas at the LaAlO<sub>3</sub>/SrTiO<sub>3</sub> Heterointerface. *Nature* **2004**, *427* (6973), 423–426. <https://doi.org/10.1038/nature02308>.
- (4) Hwang, H. Y.; Iwasa, Y.; Kawasaki, M.; Keimer, B.; Nagaosa, N.; Tokura, Y. Emergent Phenomena at Oxide Interfaces. *Nature Mater* **2012**, *11* (2), 103–113. <https://doi.org/10.1038/nmat3223>.
- (5) Zubko, P.; Gariglio, S.; Gabay, M.; Ghosez, P.; Triscone, J.-M. Interface Physics in Complex Oxide Heterostructures. *Annu. Rev. Condens. Matter Phys.* **2011**, *2* (1), 141–165. <https://doi.org/10.1146/annurev-conmatphys-062910-140445>.

- (6) Fullerton, E. E.; Jiang, J. S.; Grimsditch, M.; Sowers, C. H.; Bader, S. D. Exchange-Spring Behavior in Epitaxial Hard/Soft Magnetic Bilayers. *Physical Review B* **1998**, *58*, 12 193-12 200.
- (7) Fullerton, E. E.; Jiang, J. S.; Bader, S. D. Hard/Soft Magnetic Heterostructures: Model Exchange-Spring Magnets. *Journal of Magnetism and Magnetic Materials* **1999**, *200* (1–3), 392–404. [https://doi.org/10.1016/S0304-8853\(99\)00376-5](https://doi.org/10.1016/S0304-8853(99)00376-5).
- (8) Thiele, J.-U.; Maat, S.; Fullerton, E. E. FeRh/FePt Exchange Spring Films for Thermally Assisted Magnetic Recording Media. *Appl. Phys. Lett.* **2003**, *82* (17), 2859–2861. <https://doi.org/10.1063/1.1571232>.
- (9) Thiele, J.-U.; Maat, S.; Robertson, J. L.; Fullerton, E. E. Magnetic and Structural Properties of FePt–FeRh Exchange Spring Films for Thermally Assisted Magnetic Recording Media. *IEEE Trans. Magn.* **2004**, *40* (4), 2537–2542. <https://doi.org/10.1109/TMAG.2004.829325>.
- (10) Li, B.; Chopdekar, R. V.; Arenholz, E.; Mehta, A.; Takamura, Y. Unconventional Switching Behavior in  $\text{La}_{0.7}\text{Sr}_{0.3}\text{MnO}_3/\text{La}_{0.7}\text{Sr}_{0.3}\text{CoO}_3$  Exchange-Spring Bilayers. *Appl. Phys. Lett.* **2014**, *105* (20), 202401. <https://doi.org/10.1063/1.4902115>.
- (11) Li, B.; Chopdekar, R. V.; N'Diaye, A. T.; Mehta, A.; Byers, J. P.; Browning, N. D.; Arenholz, E.; Takamura, Y. Tuning Interfacial Exchange Interactions via Electronic Reconstruction in Transition-Metal Oxide Heterostructures. *Appl. Phys. Lett.* **2016**, *109* (15), 152401. <https://doi.org/10.1063/1.4964407>.

- (12) Kane, A. M.; Chopdekar, R. V.; N'Diaye, A. T.; Scholl, A.; Arenholz, E.; Mehta, A.; Takamura, Y. Decoupling Exchange Bias and Coercivity Enhancement in a Perovskite Oxide Exchange Spring Bilayer. *Phys. Rev. Materials* **2019**, *3* (1), 014413. <https://doi.org/10.1103/PhysRevMaterials.3.014413>.
- (13) Lauter-Pasyuk, V. Neutron Grazing Incidence Techniques for Nano-Science. *Collection SFN* **2007**, *7*, 221–240.
- (14) Blundell, S. J.; Bland, J. A. C. Polarized Neutron Reflection as a Probe of Magnetic Films and Multilayers. *Phys. Rev. B* **1992**, *46* (6), 3391–3400. <https://doi.org/10.1103/PhysRevB.46.3391>.
- (15) Toperverg, B. P. Polarized Neutron Reflectometry of Magnetic Nanostructures. *Phys. Metals Metallogr.* **2015**, *116* (13), 1337–1375. <https://doi.org/10.1134/S0031918X15130025>.
- (16) Ankner, J. F.; Felcher, G. P. Polarized-Neutron Reflectometry. *Journal of Magnetism and Magnetic Materials* **1999**, *14*.
- (17) Liu, Y.; te Velthuis, S. G. E.; Jiang, J. S.; Choi, Y.; Bader, S. D.; Parizzi, A. A.; Ambaye, H.; Lauter, V. Magnetic Structure in Fe/Sm-Co Exchange Spring Bilayers with Intermixed Interfaces. *Phys. Rev. B* **2011**, *83* (17), 174418. <https://doi.org/10.1103/PhysRevB.83.174418>.
- (18) O'Donovan, K. V.; Borchers, J. A.; Maat, S.; Carey, M. J.; Gurney, B. A. Neutron Reflectivity on CoFe<sub>2</sub>O<sub>4</sub> Exchange Springs for Spin Valve Applications. *Journal of Applied Physics* **2004**, *95* (11), 7507–7509. <https://doi.org/10.1063/1.1669127>.

(19) Lauter-Pasyuk, V.; Lauter, H. J.; Toperverg, B.; Nikonov, O.; Kravtsov, E.; Romashev, L.; Ustinov, V. Magnetic Neutron Off-Specular Scattering for the Direct Determination of the Coupling Angle in Exchange-Coupled Multilayers. *Journal of Magnetism and Magnetic Materials* **2001**, *3*.

(20) O'Donovan, K. V.; Borchers, J. A.; Majkrzak, C. F.; Hellwig, O.; Fullerton, E. E. Pinpointing Chiral Structures with Front-Back Polarized Neutron Reflectometry. *Phys. Rev. Lett.* **2002**, *88* (6), 067201. <https://doi.org/10.1103/PhysRevLett.88.067201>.

(21) Hoffman, J. D.; Kirby, B. J.; Kwon, J.; Fabbris, G.; Meyers, D.; Freeland, J. W.; Martin, I.; Heinonen, O. G.; Steadman, P.; Zhou, H.; Schlepütz, C. M.; Dean, M. P. M; te Velthuis, S. G. E.; Zuo, J.-M.; Bhattacharya, A. Oscillatory Noncollinear Magnetism Induced by Interfacial Charge Transfer in Superlattices Composed of Metallic Oxides. *Phys. Rev. X* **2016**, *6* (4), 041038. <https://doi.org/10.1103/PhysRevX.6.041038>.

(22) Hoffman, J. D.; Wu, S. M.; Kirby, B. J.; Bhattacharya, A. Tunable Noncollinear Antiferromagnetic Resistive Memory through Oxide Superlattice Design. *Phys. Rev. Applied* **2018**, *9* (4), 044041. <https://doi.org/10.1103/PhysRevApplied.9.044041>.

(23) Walter, J.; Yu, G.; Yu, B.; Grutter, A.; Kirby, B.; Borchers, J.; Zhang, Z.; Zhou, H.; Birol, T.; Greven, M.; Leighton, C. Ion-Gel-Gating-Induced Oxygen Vacancy Formation in Epitaxial  $\text{La}_{0.5}\text{Sr}_{0.5}\text{CoO}_{3-\delta}$  Films from *in Operando* x-Ray and Neutron Scattering. *Phys. Rev. Materials* **2017**, *1* (7), 071403. <https://doi.org/10.1103/PhysRevMaterials.1.071403>.

(24) Gilbert, D. A.; Grutter, A. J.; Murray, P. D.; Chopdekar, R. V.; Kane, A. M.; Ionin, A. L.; Lee, M. S.; Spurgeon, S. R.; Kirby, B. J.; Maranville, B. B.; N'Diaye, A. T.; Mehta, A.;

Arenholz, E.; Liu, K.; Takamura, Y.; Borchers, J. A. Ionic Tuning of Cobaltites at the Nanoscale. *Phys. Rev. Materials* **2018**, *2* (10), 104402. <https://doi.org/10.1103/PhysRevMaterials.2.104402>.

(25) Rippey, G.; Trinh, L.; Kane, A. M.; Ionin, A. L.; Lee, M. S.; Chopdekar, R. V.; Christiansen-Salameh, J. M.; Gilbert, D. A.; Grutter, A. J.; Murray, P. D.; Holt, M. V.; Cai, Z.; Liu, K.; Takamura, Y.; Kukreja, R. X-Ray Nanodiffraction Studies of Ionically Controlled Nanoscale Phase Separation in Cobaltites. *Phys. Rev. Materials* **2019**, *3* (8), 082001. <https://doi.org/10.1103/PhysRevMaterials.3.082001>.

(26) Kemik, N.; Gu, M.; Yang, F.; Chang, C.-Y.; Song, Y.; Bibee, M.; Mehta, A.; Biegalski, M. D.; Christen, H. M.; Browning, N. D.; Takamura, Y. Resonant X-Ray Reflectivity Study of Perovskite Oxide Superlattices. *Appl. Phys. Lett.* **2011**, *99* (20), 201908. <https://doi.org/10.1063/1.3660719>.

(27) Björck, M.; Andersson, G. *GenX*: An Extensible X-Ray Reflectivity Refinement Program Utilizing Differential Evolution. *J Appl Crystallogr* **2007**, *40* (6), 1174–1178. <https://doi.org/10.1107/S0021889807045086>.

(28) Lee, J.-S.; Arena, D. A.; Yu, P.; Nelson, C. S.; Fan, R.; Kinane, C. J.; Langridge, S.; Rossell, M. D.; Ramesh, R.; Kao, C.-C. Hidden Magnetic Configuration in Epitaxial  $\text{La}_{1-x}\text{Sr}_x\text{MnO}_3$  Films. *Phys. Rev. Lett.* **2010**, *105* (25), 257204. <https://doi.org/10.1103/PhysRevLett.105.257204>.

(29) Bianconi, A.; Jackson, D.; Monahan, K. Intrinsic Luminescence Excitation Spectrum and Extended X-Ray Absorption Fine Structure above the K Edge in  $\text{CaF}_2$ . *Phys. Rev. B* **1978**, *17* (4), 2021–2024. <https://doi.org/10.1103/PhysRevB.17.2021>.

- (30) Lauter, V.; Ambaye, H.; Goyette, R.; Hal Lee, W.-T.; Parizzi, A. Highlights from the Magnetism Reflectometer at the SNS. *Physica B: Condensed Matter* **2009**, *404* (17), 2543–2546. <https://doi.org/10.1016/j.physb.2009.06.021>.
- (31) Leptos Manual. Bruker AXS, W. 2005. Re: author request for this reference, this is a software manual with no listed author.
- (32) Chopdekar, R. V.; Arenholz, E.; Suzuki, Y. Orientation and Thickness Dependence of Magnetization at the Interfaces of Highly Spin-Polarized Manganite Thin Films. *Phys. Rev. B* **2009**, *79* (10), 104417. <https://doi.org/10.1103/PhysRevB.79.104417>.
- (33) Ott, F.; Viret, M.; Borges, R.; Lyonnet, R.; Jacquet, E.; Fermon, C. Interface Magnetism of La<sub>0.7</sub>Sr<sub>0.3</sub>MnO<sub>3</sub> Thin Films Studied by Neutron Reflectometry. *Journal of Magnetism and Magnetic Materials* **2000**, *211*, 200–205.
- (34) Verna, A.; Davidson, B. A.; Szeto, Y.; Petrov, A. Yu.; Mirone, A.; Giglia, A.; Mahne, N.; Nannarone, S. Measuring Magnetic Profiles at Manganite Surfaces with Monolayer Resolution. *Journal of Magnetism and Magnetic Materials* **2010**, *322* (9–12), 1212–1216. <https://doi.org/10.1016/j.jmmm.2009.05.022>.
- (35) Grutter, A. J.; Gilbert, D. A.; Alaan, U. S.; Arenholz, E.; Maranville, B. B.; Borchers, J. A.; Suzuki, Y.; Liu, K.; Kirby, B. J. Reversible Control of Magnetism in La<sub>0.67</sub>Sr<sub>0.33</sub>MnO<sub>3</sub> through Chemically-Induced Oxygen Migration. *Appl. Phys. Lett.* **2016**, *108* (8), 082405. <https://doi.org/10.1063/1.4942645>.

- (36) Guo, E.-J.; Charlton, T.; Ambaye, H.; Desautels, R. D.; Lee, H. N.; Fitzsimmons, M. R. Orientation Control of Interfacial Magnetism at  $\text{La}_{0.67}\text{Sr}_{0.33}\text{MnO}_3/\text{SrTiO}_3$  Interfaces. *ACS Appl. Mater. Interfaces* **2017**, *9* (22), 19307–19312. <https://doi.org/10.1021/acsami.7b03252>.
- (37) Smadici, Ş.; Abbamonte, P.; Bhattacharya, A.; Zhai, X.; Jiang, B.; Rusydi, A.; Eckstein, J. N.; Bader, S. D.; Zuo, J.-M. Electronic Reconstruction at  $\text{SrMnO}_3 - \text{LaMnO}_3$  Superlattice Interfaces. *Phys. Rev. Lett.* **2007**, *99* (19), 196404. <https://doi.org/10.1103/PhysRevLett.99.196404>.
- (38) Shannon, R. D.; Prewitt, C. T. Effective Ionic Radii in Oxides and Fluorides. *Acta Crystallogr B Struct Sci* **1969**, *25* (5), 925–946. <https://doi.org/10.1107/S0567740869003220>.
- (39) Shannon, R. D. Revised Effective Ionic Radii and Systematic Studies of Interatomic Distances in Halides and Chalcogenides. *Acta Crystallographica* **1976**, *A32*, 751–767.
- (40) Zuev, A.; Vylkov, A.; Petrov, A.; Tsvetkov, D. Defect Structure and Defect-Induced Expansion of Undoped Oxygen Deficient Perovskite  $\text{LaCoO}_{3-\delta}$ . *Solid State Ionics* **2008**, *179* (33–34), 1876–1879. <https://doi.org/10.1016/j.ssi.2008.06.001>.
- (41) Liu, B.; Wang, Y.; Liu, G.; Feng, H.; Yang, H.; Xue, X.; Sun, J. Tuning the Magnetic Properties of  $\text{La}_{0.67}\text{Sr}_{0.33}\text{CoO}_{3-\delta}$  Films by Oxygen Pressure. *Phys. Rev. B* **2016**, *93* (9), 094421. <https://doi.org/10.1103/PhysRevB.93.094421>.
- (42) Zuev, A. Yu.; Tsvetkov, D. S. Oxygen Nonstoichiometry, Defect Structure and Defect-Induced Expansion of Undoped Perovskite  $\text{LaMnO}_{3\pm\delta}$ . *Solid State Ionics* **2010**, *181* (11–12), 557–563. <https://doi.org/10.1016/j.ssi.2010.02.024>.

- (43) Kienzle, P. Neutron Activation and Scattering Calculator  
<https://www.ncnr.nist.gov/resources/activation/> (accessed Jun 10, 2019).
- (44) Li, B.; Chopdekar, R. V.; Kane, A. M.; Hoke, K.; N'Diaye, A. T.; Arenholz, E.; Takamura, Y. Thickness-Dependent Magnetic and Electrical Transport Properties of Epitaxial  $\text{La}_{0.7}\text{Sr}_{0.3}\text{CoO}_3$  Films. *AIP Advances* **2017**, 7 (4), 045003. <https://doi.org/10.1063/1.4979921>.
- (45) Ji, Y.; Chien, C. L.; Tomioka, Y.; Tokura, Y. Measurement of Spin Polarization of Single Crystals of  $\text{La}_{0.7}\text{Sr}_{0.3}\text{MnO}_3$  and  $\text{La}_{0.6}\text{Sr}_{0.4}\text{MnO}_3$ . *Phys. Rev. B* **2002**, 66 (1), 012410. <https://doi.org/10.1103/PhysRevB.66.012410>.
- (46) Torija, M. A.; Sharma, M.; Gazquez, J.; Varela, M.; He, C.; Schmitt, J.; Borchers, J. A.; Laver, M.; El-Khatib, S.; Leighton, C. Chemically Driven Nanoscopic Magnetic Phase Separation at the  $\text{SrTiO}_3(001)/\text{La}_{1-x}\text{Sr}_x\text{CoO}_3$  Interface. *Adv. Mater.* **2011**, 23 (24), 2711–2715. <https://doi.org/10.1002/adma.201100417>.
- (47) Hemberger, J.; Krimmel, A.; Kurz, T.; Krug von Nidda, H.-A.; Ivanov, V. Yu.; Mukhin, A. A.; Balbashov, A. M.; Loidl, A. Structural, Magnetic, and Electrical Properties of Single-Crystalline  $\text{La}_{1-x}\text{Sr}_x\text{MnO}_3$  ( $0.4 < x < 0.85$ ). *Phys. Rev. B* **2002**, 66 (9), 094410. <https://doi.org/10.1103/PhysRevB.66.094410>.
- (48) Sakai, J.; Ito, N.; Imai, S. Oxygen Content of  $\text{La}_{1-x}\text{Sr}_x\text{MnO}_{3-y}$  Thin Films and Its Relation to Electric-Magnetic Properties. *Journal of Applied Physics* **2006**, 99 (8), 08Q318. <https://doi.org/10.1063/1.2176323>.

(49) Urushibara, A.; Moritomo, Y.; Arima, T.; Asamitsu, A.; Kido, G.; Tokura, Y. Insulator-Metal Transition and Giant Magnetoresistance in  $\text{La}_{1-x}\text{Sr}_x\text{MnO}_3$ . *Phys. Rev. B* **1995**, *51* (20), 14103–14109. <https://doi.org/10.1103/PhysRevB.51.14103>.

(50) Gazquez, J.; Bose, S.; Sharma, M.; Torija, M. A.; Pennycook, S. J.; Leighton, C.; Varela, M. Lattice Mismatch Accommodation via Oxygen Vacancy Ordering in Epitaxial  $\text{La}_{0.5}\text{Sr}_{0.5}\text{CoO}_{3-\delta}$  Thin Films. *APL Materials* **2013**, *1* (1), 012105. <https://doi.org/10.1063/1.4809547>.